Int. J. Solids Structures, 1978, Vol. 14, pp. 39–51. Pergamon Press. Printed in Great Britain

PROPAGATION OF WEAK WAVES IN ELASTIC-PLASTIC AND ELASTIC-VISCOPLASTIC SOLIDS WITH INTERFACES

BHARAT BHUSHAN† and W. E. JAHSMAN
Department of Mechanical Engineering, University of Colorado, Boulder, CO 80309, U.S.A.

(*Received* 20 *May* 1977; *revised* 13 *July* 1977)

Abstract—A numerical technique based on the method of singular surfaces has been developed for the computation of wave propagation in solids exhibiting rate-independent elastic-plastic or rate-dependent elastic-viscoplastic behavior. The von Mises yield condition and associated flow rule is taken to represent the rate-independent behavior, while the Perzyna dynamic overstress model is taken to represent the rate-dependent behavior. For 1100–0 Al, a good empirical fit with published experimental data was found to be:

$$J_2^{1/2} - \kappa(W^p) = (\tau_0/\gamma_0)(\dot{W}^p/J_2^{1/2})$$

where: J_2 is the second invariant of the stress deviator; $\kappa(W^p)$ is the static hardening curve; W^p is the plastic work and the parameter $(\tau_0/\gamma_0) = 0$ (rate-independent model) or $(80)^{-1}$ to $(70)^{-1}$ MPa·s. In the numerical technique, the "connection equations" which provide relations between discontinuities in space and time derivatives lend themselves naturally to finite difference representations. A five-point space-time grid (center point coincident with the instantaneous location of the singular surface) is sufficient for the differenced form of the connection equations and suggests a natural marching scheme for the calculation of all necessary variables at each time step. Supplementing these equations which hold in the interior of the specimen are interface equations which assure continuity in stress and velocity across boundaries which separate materials with dissimilar properties. Application of the technique is made to wave propagation in pure shear for the purpose of comparing numerical predictions with relevant experimental data. The measurements of Duffy *et al.*[10] which are obtained from the torsional Kolsky apparatus (one dimensional torsional shear wave propagation in a thin-walled tube) were compared with predictions obtained numerically. By using the experimental input pulse history and the constitutive equation reported above, excellent agreement between the predicted and observed histories of reflected and transmitted pulses was obtained when the viscoplastic model was used. Poorer agreement was observed when the rate-independent model $(\tau_0/\gamma_0 = 0)$ was used. It is concluded that the Perzyna model gives good results for the behavior of 1100–0 Al at high rates of strain.

1. INTRODUCTION

Analysis of inelastic wave propagation has been of great interest in many fields, e.g. nuclear explosions and structures under dynamic loads. Several techniques have been used to study the general wave propagation problem. Von Neumann and Richtmyer[1] used finite differenced hydrodynamic equations with artificial viscosity to study one-dimensional shock wave propagation. Courant and Friedrichs[2] described the method of characteristics and illustrated several applications including wave propagation in solids. Later, one- and two-dimensional wave propagation computer programs using finite difference approximations were developed at Sandia Laboratories[3, 4] to study material behavior.

Singular surface theory has been developed by many workers, e.g. see Hill[5] and Janssen *et al.*[6]. The interface conditions using singular surfaces were developed by Jahsman[7]. However, the singular surface approach has never been put to numerical use. The purpose of this paper is to describe the numerical program based on the singular surface approach and to apply the program thus developed to the propagation of weak waves through an inelastic specimen sandwiched between two elastic bars (the Kolsky apparatus).

2. SINGULAR SURFACE RELATIONS

Time and space derivatives $\mathring{h}$ and $h_{,i}$ of any function h may be expressed in terms of derivatives written with respect to local coordinates (ξ_α, n) etched on and normal to the moving

†Presently at: Mechanical Technology Incorporated, 968 Albany-Shaker Road, Latham, NY 12110, U.S.A.

singular surface $\Sigma(t)$ (Fig. 1) as follows:

$$\mathring{h} = \frac{\delta h}{\delta t} - \left(c_\alpha \frac{\partial h}{\partial \xi_\alpha} + c_n \frac{\partial h}{\partial n} \right) \quad (\alpha = 1, 2) \tag{1}$$

$$h_{,i} = \frac{\partial h}{\partial \xi_\alpha} \xi_{\alpha,i} + \frac{\partial h}{\partial n} n_i \quad (i = 1, 2, 3). \tag{2}$$

The operator $\delta/\delta t$ represents the time derivative recorded by an observer moving with Σ, and (c_α, c_n) are the components of the velocity of the surface Σ. The component of the normal to Σ in the x_i direction is n_i. When Σ admits discontinuities in the derivatives of h across it ("weak waves"), eqns (1) and (2), when written immediately ahead of and behind Σ and then differenced, reduce to

$$[\mathring{h}] = -c_n \left[\frac{\partial h}{\partial n} \right] \tag{3}$$

$$[h_{,i}] = \left[\frac{\partial h}{\partial n} \right] n_i. \tag{4}$$

Brackets denote the differencing operation described above. Additional details may be found in Ref. [6]. The simplification results from the fact that h itself is continuous so that $[h] = 0$, $[\delta h/\delta t] = \delta[h]/\delta t = 0$ and $[\partial h/\partial \xi_\alpha] = \partial[h]/\partial \xi_\alpha = 0$. Retained in this operation is the discontinuity in the normal derivative of h across Σ.

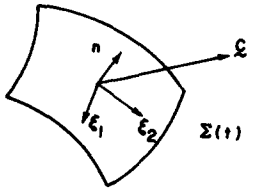

Fig. 1. Singular surface and co-ordinates.

3. CONSTITUTIVE EQUATIONS

When the strain rate tensor $\mathring{\epsilon}_{ij}$ can be decomposed into its elastic and plastic parts

$$\mathring{\epsilon}_{ij} = \mathring{\epsilon}^e_{ij} + \mathring{\epsilon}^p_{ij}, \tag{5}$$

the elastic and plastic consititutive equations may be considered separately. For an isotropic elastic material, the familiar relation

$$\epsilon^e_{ij} = \frac{1}{2G} s_{ij} + \frac{1}{3K} \sigma \delta_{ij} \tag{6}$$

is used (G and K are the shear and bulk moduli, respectively). Components of the stress tensor σ_{ij} and stress deviator tensor s_{ij} are related through

$$s_{ij} = \sigma_{ij} - \sigma \delta_{ij} \tag{7}$$

and $\sigma \equiv \sigma_{kk}/3$ is the mean stress. The Kronecker delta is given by δ_{ij}.

For an isotropic plastic material, the general form of the consititutive relation

$$\mathring{\epsilon}^p_{ij} = \begin{cases} \mathring{\Lambda} \dfrac{\partial f}{\partial \sigma_{ij}}, & \mathring{W}^p > 0 \\ 0, & \mathring{W}^p = 0 \end{cases} \tag{8}$$

is the same for both rate-independent (classical plasticity) and visco-plastic behavior. Here, $\mathring{W}^p = s_{ij}\mathring{\epsilon}^p_{ij}$ is the plastic power (time rate of change of the plastic work, $W^p = \int s_{ij}\, \mathrm{d}\epsilon^p_{ij}$), and $f = f(\sigma_{ij}, \epsilon^p_{ij})$ is the instantaneous yield surface. The relationship between the parameter $\mathring{\Lambda}$ and $\mathring{W}^p$ and f is obtained by multiplying eqn (8) by s_{ij} and summing:

$$\mathring{\Lambda} = \mathring{W}^p / \sigma_{kl}(\partial f / \partial \sigma_{kl}) \tag{9}$$

Quite different characteristics are exhibited by eqn (8) depending on the form of $\mathring{\Lambda}$ (or f). In the rate-independent theory,

$$f = \kappa(W^p), \tag{10}$$

κ is the hardening function and depends solely on plastic work. Differentiation of eqn (10) with respect to time then provides a linear relationship between $\mathring{W}^p$, $\mathring{\sigma}_{ij}$ and $\mathring{\epsilon}^p_{ij}$:

$$\mathring{W}^p = [(\partial f / \partial \sigma_{ij})\mathring{\sigma}_{ij} + (\partial f / \partial \epsilon^p_{ij})\mathring{\epsilon}^p_{ij}]/(\mathrm{d}\kappa / \mathrm{d}W^p). \tag{11}$$

On the other hand, the Perzyna model[8] of viscoplastic behavior introduces the following expression for $\mathring{\Lambda}$:

$$\mathring{\Lambda} = \gamma_0 \langle \dot{\Phi}(F) \rangle \tag{12}$$

where γ_0 is the viscoplastic constant for the material and $\Phi(F)$ is a monotonic function of the dynamic overstress function F, defined as

$$F = (f - \kappa)/\tau_0 \tag{13}$$

where τ_0 is the initial static yield strength in pure shear ($=\kappa(0)$, by definition). Thus, the viscoplastic model permits an instantaneous yield function in excess of the static hardening function (thus, eqn (13) replaces eqn (10)). The brackets on Φ denote

$$\langle \Phi \rangle = \begin{cases} 0, & \Phi < 0 \\ \Phi, & \Phi \geq 0 \end{cases} \tag{14}$$

and distinguish loading from unloading provided $\Phi(0) = 0$ since $\Phi \lesseqgtr 0$ implies $F \lesseqgtr 0$ because of the monotonicity of Φ. If eqns (9), (12) and (13) are combined, a new equation for plastic power replaces eqn (11):

$$\mathring{W}^p = \sigma_{kl}(\partial f / \partial \sigma_{kl})\gamma_0 \langle \Phi((f - \kappa)/\tau_0) \rangle. \tag{15}$$

No longer does plastic power depend linearly on $\mathring{\sigma}_{ij}$ and $\mathring{\epsilon}^p_{ij}$; instead, it depends on the functions themselves (σ_{ij} and ϵ^p_{ij}) and on plastic work W^p.

If the derivative discontinuity in plastic strain rate across a singular surface $\Sigma(t)$ (Section 2) is of interest, we note from eqn (8) that $[\mathring{\epsilon}^p_{ij}] \neq 0$ only if $[\mathring{\Lambda}] \neq 0$ since $\partial f / \partial \sigma_{ij}$ depends only on σ_{ij} and ϵ^p_{ij}. Further, by inspection of eqn (9), this condition can be satisfied only if $[\mathring{W}^p] \neq 0$ when either (or both) $[\mathring{\sigma}_{ij}]$ and $[\mathring{\epsilon}^p_{ij}] \neq 0$ (eqn 11); however, for viscoplastic behavior, $[\mathring{W}^p] = 0$ since the right-hand side of eqn (15) contains no derivatives. Thus, the viscoplastic model of Perzyna does not admit the propagation of derivative discontinuities in ϵ^p_{ij}. Only the elastic part of the strain rate tensor can be discontinuous across $\Sigma(t)$.

As a special case of $f(\sigma_{ij}, \epsilon^p_{ij})$ and $\Phi(F)$, we take

$$f = \left(\frac{1}{2} s_{ij} s_{ij}\right)^{1/2} \tag{16}$$

$$\Phi = F. \tag{17}$$

Although other choices have also been proposed by Perzyna[8], the equations above represent the simplest forms which show acceptable agreement with experimental data. The form of f given in eqn (16) corresponds to the von Mises yield condition, and in one-dimensional problems the form of Φ given in eqn (17) corresponds to that used by Malvern[9]. Since $1/2 s_{ij}s_{ij} = J_2$, the second invariant of the stress deviator tensor, eqns (16) and (17), in conjunction with eqn (15), reduce to:

$$J_2^{1/2} = \kappa(W^p) + (\tau_0/\gamma_0)(\mathring{W}^p/J_2^{1/2}). \tag{18}$$

The experimental data for Al 1100–0 as reported in [10–14] were obtained from a number of tests using the Kolsky apparatus[15] (split Hopkinson pressure bar or torsional thin-walled tube). The data were reduced to hardening curves $\tau = \tau(W^P, \mathring{W}^P)$, using the standard Kolsky formulas[15] which provide approximate expressions for average stress and average strain rate in the specimen. A good fit between the predicted behavior given by eqn (18) and the experimental data was obtained by choosing $(\tau_0/\gamma_0) = (70)^{-1}$ MPa·s. Comparison between measurements and predictions is shown in Fig. 2.

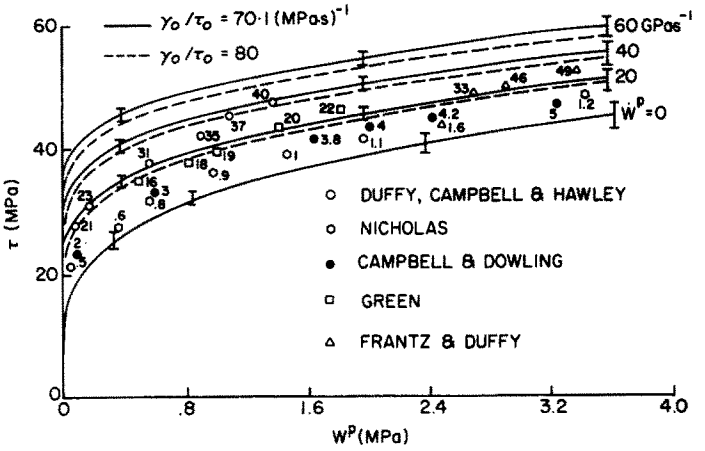

Fig. 2. $\tau - W^P$ curves for Al 1100–0.

4. SHEAR WAVE PROPAGATION

When the material is in a state of simple shear, the general momentum conservation equations

$$\sigma_{ji,j} - \rho \mathring{v}_i = 0 \tag{19}$$

and the kinematic conditions

$$\mathring{\epsilon}_{ij} - \frac{1}{2}(v_{i,j} + v_{j,i}) = 0 \tag{20}$$

(where v_i are the components of particle velocity and ρ is the constant mass density of the material) simplify considerably. Letting $x_3 = z$ be the (axial) direction of wave propagation, we can write

$$\begin{aligned} &\sigma_{11} = \sigma_{22} = \sigma_{33} = 0 \\ &\sigma_{12} = \sigma_{13} = 0 \\ &\sigma_{23} = \tau \end{aligned} \tag{21}$$

$$\begin{aligned} &v_1 = v_3 = 0 \\ &v_2 = v. \end{aligned} \tag{22}$$

The non-zero components of eqns (19) and (20) are then

$$\tau' - \rho\mathring{v} = 0 \tag{23}$$

$$\mathring{\gamma} - \frac{1}{2}v' = 0 \tag{24}$$

where prime denotes differentiation with respect to z and $\mathring{\gamma}$ is the total shear strain rate

$$\begin{aligned} \mathring{\gamma} &= \mathring{\gamma}^e + \mathring{\gamma}^p \\ \gamma^e &= \frac{1}{2G}\tau \end{aligned} \tag{25}$$

(see eqns (5) and (6)). Since $\mathring{W}^p = 2\tau\,\mathring{\gamma}^p$ and $\mathring{W}$ (total power density) $= 2\tau\,\mathring{\gamma}$, eqns (24) and (25) become

$$\begin{aligned} \mathring{W} &= \tau v' \\ \mathring{W} &= \frac{1}{G}\tau\mathring{\tau} + \mathring{W}^p \end{aligned} \tag{26}$$

or, through subtraction,

$$\frac{1}{G}\tau\mathring{\tau} = \tau v' - \mathring{W}^p \tag{27}$$

When the material is rate-independent and yields according to the von Mises criterion (see eqns (10) and (16)), $f = J_2^{1/2} = |\tau| = \kappa(W^p)$ so that

$$\mathring{W}^p = \frac{\mathring{\tau}\,\mathrm{sgn}(\tau)}{\mathrm{d}\kappa/\mathrm{d}W^p}, \quad \text{(rate-independent)}. \tag{28}$$

For the rate-dependent material governed by the Perzyna equation (eqn 18),

$$\mathring{W}^p = |\tau|\frac{|\tau| - \kappa}{(\tau_0/\gamma_0)}. \tag{29}$$

Equations (28) and (29) are valid when $\mathring{W}^p \geq 0$; otherwise (i.e. $\mathring{\tau}\,\mathrm{sgn}(\tau) < 0$ or $|\tau| < \kappa$), $\mathring{W}^p \equiv 0$ in eqn (27).

Equation (25) brings out clearly the fact that for stresses below the static strength ($|\tau| < \kappa$), the shear stress and strain rates are linearly related. When the shear stress reaches this level, the plastic power is proportional to the shear stress rate (rate-independent material, eqn (28)). If the material behavior is viscoplastic, the shear stress may exceed the static strength, and the plastic power is proportional to the dynamic overstress (eqn (29)).

5. INTERFACE CONDITIONS

Consider two shear waves, one right traveling (RT) in a medium designated $-$ and the other left traveling (LT) in medium designated $+$, which encounter an interface separating the $-$ and $+$ media. As a result of this encounter, reflected and transmitted waves will be generated at the interface to insure continuity in stress and velocity across the interface (welded contact). By analogy to the equations developed early by Jahsman[7], the continuity conditions at the interface may be written as:

$$\begin{aligned} [\mathring{\tau}]_{RT-} + [\mathring{\tau}]_{LT-} &= [\mathring{\tau}]_{RT+} + [\mathring{\tau}]_{LT+} \\ [\mathring{v}]_{RT-} + [\mathring{v}]_{LT-} &= [\mathring{v}]_{RT+} + [\mathring{v}]_{LT+}. \end{aligned} \tag{30}$$

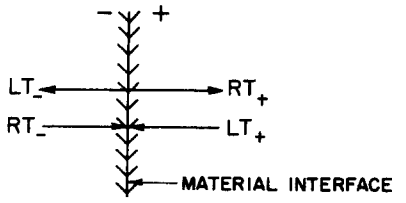

Fig. 3. Incident, reflected and transmitted waves at a material interface.

The first and last terms in each of eqns (30) represent the contributions of the right- and left-traveling waves which are incident on the interface; the remaining terms represent the contributions of the reflected and transmitted waves, respectively. Figure 3 illustrates the four waves at the interface.

Discontinuities in $\mathring{\tau}$ and $\mathring{v}$ are introduced in eqn (30) for compatibility with eqn (23) in conjunction with eqns (3) and (4). Note that continuity in τ and v is automatically assured through the application of eqns (3) and (4) which depend on the "weak wave" requirement that $[\tau] = [v] = 0$.

By virtue of the kinematic equations (eqns (3) and (4)), we may write:

$$[\mathring{\tau}]_{\substack{RT \\ LT}} = \mp c[\tau']_{\substack{RT \\ LT}} \tag{31}$$

where increasing z and t correspond to the direction of a right-traveling wave. The wave speed c is determined from the consititutive equations, and explicit forms for classical elastic-plastic and visco-plastic materials are provided in Section 6.

Completing the set of equations necessary for the interface relations are the derivative discontinuity forms of eqn (23):

$$[\tau']_{\substack{RT \\ LT}} = \rho[\mathring{v}]_{\substack{RT \\ LT}} \tag{32}$$

The two waves represented by eqn (32) may be added to obtain a discontinuity relation of the same structure without subscripts.

By regarding the incident waves (denoted by $[\ ]_{RT-}$ and $[\ ]_{LT+}$) as known quantities, we may solve for the variables associated with the reflected and transmitted waves ($[\ ]_{LT-}$ and $[\ ]_{RT+}$) in terms of these known variables by combining eqns (30)–(32). In terms of $[\mathring{\tau}]_{\substack{RT- \\ LT+}}$, $[\mathring{\tau}]_{\substack{LT- \\ RT+}}$ becomes

$$[\mathring{\tau}]_{LT-} = \frac{(\rho c)_+/(\rho c)_- - 1}{(\rho c)_+/(\rho c)_- + 1}[\mathring{\tau}]_{RT-} + \frac{2(\rho c)_-/(\rho c)_+}{(\rho c)_-/(\rho c)_+ + 1}[\mathring{\tau}]_{LT+}$$

$$[\mathring{\tau}]_{RT+} = \frac{2(\rho c)_+/(\rho c)_-}{(\rho c)_+/(\rho c)_- + 1}[\mathring{\tau}]_{RT-} + \frac{(\rho c)_-/(\rho c)_+ - 1}{(\rho c)_-/(\rho c)_+ + 1}[\mathring{\tau}]_{LT+}. \tag{33}$$

Expressions for $[\mathring{v}]_{\substack{LT- \\ RT+}}$ are then easily determined from $[\mathring{\tau}]_{\substack{LT- \\ RT+}}$ simply by eqns (31) and (32).

$$[\mathring{v}]_{\substack{RT \\ LT}} = \mp \frac{1}{\rho c}[\mathring{\tau}]_{\substack{RT \\ LT}}. \tag{34}$$

Note that eqn (34) may also be used to replace $[\mathring{\tau}]_{\substack{RT- \\ LT+}}$ with $[\mathring{v}]_{\substack{RT- \\ LT+}}$ in eqns (33) if velocity is the more convenient variable to be used with the incident wave. When the material behavior is elastic, the wave speed c is constant, and the acoustic impedances $(\rho c)_\pm$ are also constant. Equations (33) may then be recognized as the familiar relations for one-dimensional waves propagating across an interface at normal incidence.

Because the experimental data used for comparison in Section 7 were obtained from a torsional Kolsky apparatus in which the specimen dimensions differed from those of the input and output bars, eqn (30) must be replaced by torque and angular velocity continuity equations.

$$[\mathring{T}]_{RT-}+[\mathring{T}]_{LT-}=[\mathring{T}]_{RT+}+[\mathring{T}]_{LT+}$$
$$[\mathring{\omega}]_{RT-}+[\mathring{\omega}]_{LT-}=[\mathring{\omega}]_{RT+}+[\mathring{\omega}]_{LT+}. \tag{35}$$

When the specimen and bars are both thin-walled tubes, torque T and angular velocity ω are related to shear stress τ and particle velocity by

$$T=rA\tau$$
$$\omega=v/r \tag{36}$$

where A is the cross-sectional area of the tube and r is the mean radius. Combining eqns (35) and (36) with eqns (31) and (32) leads to a set of equations to replace eqn (33).

$$[\mathring{\tau}]_{LT-}=\frac{(\rho c)_+/(\rho c)_- -(r^2A)_-/(r^2A)_+}{(\rho c)_+/(\rho c)_- +(r^2A)_+/(r^2A)_-}[\mathring{\tau}]_{RT-}+\frac{(rA)_+}{(rA)_-}\frac{2(\rho c)_-/(\rho c)_+}{(\rho c)_-/(\rho c)_+ +(r^2A)_+/(r^2A)_-}[\mathring{\tau}]_{LT+}$$
$$[\mathring{\tau}]_{RT+}=\frac{(rA)_-}{(rA)_+}\frac{2(\rho c)_+/(\rho c)_-}{(\rho c)_+/(\rho c)_- +(r^2A)_-/(r^2A)_+}[\mathring{\tau}]_{RT-}+\frac{(\rho c)_-/(\rho c)_+ -(r^2A)_+/(r^2A)_-}{(\rho c)_-/(\rho c)_+ +(r^2A)_+/(r^2A)_-}[\mathring{\tau}]_{LT+}. \tag{37}$$

Imposing dimensional continuity across the interface eqn (37) reduces to eqn (33).

For numerical stability of the calculations for the rate-independent solid, it was found necessary to perform the differencing in eqns (34) and (37) on the product of the acoustic impedance ρc with the derivative discontinuity rather than on the latter factor alone. In the limit $(\Delta z\to 0, \Delta t\to 0)$ there will be no difference between $[\rho c\mathring{v}]$ and $\rho c[\mathring{v}]$ since ρ and c are continuous Clearly, a numerical smoothing was achieved through the use of the former expression, and it was retained for this reason.

6. NUMERICAL COMPUTATIONS

The computational scheme presented here depends on the ability to write derivative discontinuity ("connection") equations of the form

$$[\mathring{A}]=[BC'] \tag{38}$$

where A and C may be any of the variables v, τ, $\mathring{W}^P$ and W^P, and B is a continuous function of these same variables. Identifying the instantaneous site of the singular surface by (z^*, t^*), we represent the temporal and spatial derivative discontinuities by

$$[\mathring{A}]\doteq\frac{A(z^*,t^*+\Delta t_+)-A(z^*,t^*)}{\Delta t_+}-\frac{A(z^*,t^*)-A(z^*,t^*-\Delta t_-)}{\Delta t_-}$$
$$[BC']\doteq\frac{1}{2}\{B(z^*+\Delta z_+,t^*)+B(z^*,t^*)\}\frac{C(z^*+\Delta z_+,t^*)-C(z^*,t^*)}{\Delta z_+}$$
$$-\frac{1}{2}\{B(z^*,t^*)+B(z^*-\Delta z_-,t^*)\}\frac{C(z^*,t^*)-C(z^*-\Delta z_-,t^*)}{\Delta z_-}. \tag{39}$$

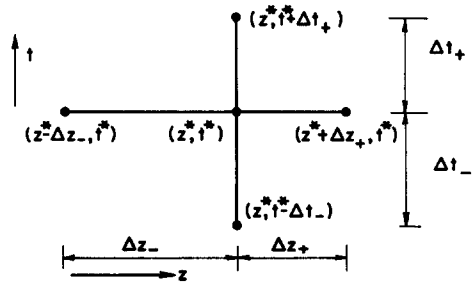

Fig. 4. Schematic of grid used with eqns (38) and (39). (Variables are known at all points except $z^*, t^*+\Delta t_+$.).

Thus, if the spatial variation of all variables is known for all times up through t^*, then eqns (38) and (39) will enable the calculation of those same variables through the new time increment Δt_+. (These equations are applicable only to interior points; i.e. points away from interfaces. Interface equations will be presented in the last part of this section.)

A visualization of the space-time grid used in the calculation of $A(z^*, t^* + \Delta t_+)$ is shown in Fig. 5. A close tie between numerical approximations for $[\mathring{A}]$ and $[C']$ and for $\overset{\circ\circ}{A}$ and C'' may be noted noted since

$$\overset{\circ\circ}{A} \doteq \frac{1}{\frac{1}{2}(\Delta t_+ + \Delta t_-)} \left\{ \frac{A(z^*, t^* + \Delta t_+) - A(z^*, t^*)}{\Delta t_+} - \frac{A(z^*, t^*) - A(z^*, t^* - \Delta t_-)}{\Delta t_-} \right\}$$

$$BC'' \doteq \frac{1}{\frac{1}{2}(\Delta z_+ + \Delta z_-)} \left[\frac{1}{2} \{B(z^* + \Delta z_+, t^*) + B(z^*, t^*)\} \frac{C(z^* + \Delta z_+, t^*) - C(z^*, t^*)}{\Delta z_+} \right.$$

$$\left. - \frac{1}{2} \{B(z^*, t^*) - B(z^* - \Delta z_-, t^*)\} \frac{C(z^*, t^*) - C(z^* - \Delta z_-, t^*)}{\Delta z_-} \right].$$

Thus, $[\mathring{A}] = [BC']$ in differenced form is indistinguishable from $\overset{\circ\circ}{A} = \bar{\dot{z}} BC''$ in differenced form when $\bar{\dot{z}}$ is interpreted as $\mathrm{d}\bar{z}/\mathrm{d}\bar{t}$, some average speed. For the special case of $C = A$, the latter equation has the form of a wave equation with $\bar{\dot{z}}B$ representing c^2, square of the wave speed.

It is convenient to let v represent the generic variable C in the equations to be presented explicitly. Then according to the kinematic equations, eqns (3) and (4), we can write a relation of the form of eqn (38) for the right- and left-traveling waves as

$$\underset{LT}{[\mathring{v}]}_{RT} = \mp c \underset{LT}{[v']}_{RT} \tag{40}$$

where the wave speed c is determined from the roots of the connection eqns (38). For the special classes of materials considered here, it may be shown that

$$c = \sqrt{(1-P)}c_2$$

$$P = \begin{cases} \left(1 + \dfrac{\kappa}{G} \dfrac{\mathrm{d}\kappa}{\mathrm{d}W^p}\right)^{-1}, & \mathring{W}^p > 0 \\ 0, & \mathring{W}^p = 0 \end{cases} \tag{41}$$

$$c_2 = \sqrt{\left(\frac{G}{\rho}\right)}$$

(rate-independent behavior), yield governed by the von Mises criterion[16], see eqn (28) or

$$c = c_2 \tag{42}$$

(viscoplastic behavior, Perzyna model). Equation (42) follows from the fact that $[\mathring{\epsilon}_{ij}^p] = 0$ (see discussion preceding eqn (16)) and thus, that all derivative discontinuities propagate at the elastic shear wave speed c_2. Although eqn (40) treats right- and left-traveling waves individually, the total contribution is merely the sum of the individual effects

$$[\mathring{v}] = [\mathring{v}]_{RT} + [\mathring{v}]_{LT}$$

$$[v'] = [v']_{RT} + [v']_{LT}. \tag{43}$$

It is the latter form, eqn (43), which is particularly useful for the computation of the other variables, although retention of the individual wave effects is necessary in dealing with the interface conditions.

Calculation of the remaining variables begins with a test of sgn $(\mathring{W}^p)$. If $|\tau| < \kappa$, $\mathring{W}^p = 0$ and

eqn (27), written in derivative discontinuity form, is used to find $\tau(z^*, t^* + \Delta t_+)$:

$$[\dot{\tau}^*] = G[v'](|\tau| < \kappa, \dot{W}^p = 0). \tag{44}$$

Since $\dot{W}^p = 0$, $W^p(z^*, t^* + \Delta t_+) = W^p(z^*, t^*)$ (no variation in W^p).

As the yield surface is broached, $|\tau| \geq \kappa$ and eqn (44) can no longer be used. Instead, the appropriate consititutive equation is put in the form represented by eqn (38). For the rate-independent material obeying the von Mises yield condition, eqn (27) in conjunction with eqn (28) gives

$$[\dot{W}^p] = \left\{\frac{(\kappa/G)\,\mathrm{sgn}(\tau)}{1 + (\kappa/G)(\mathrm{d}\kappa/\mathrm{d}W^p)}\right\} G[v'] \quad (|\tau| = \kappa, \dot{W}^p > 0). \tag{45}$$

Once $W^p(z^*, t^* + \Delta t_+)$ is obtained, $\tau(z^*, t^* + \Delta t_+)$ is found from the constitutive equation $|\tau| = \kappa(W^p)$.

When the material is viscoplastic $[\dot{W}^p] = 0$, as discussed in Section 3. Since the equation requires a constant plastic work rate across the singular surface, it is replaced by a two-term Taylor's series expansion of $\dot{W}^p(z^*, t^*)$ to provide $W^p(z^*, t^* + \Delta t_+)$

$$W^p(z^*, t^* + \Delta t_+) = W^p(z^*, t^*) + \dot{W}^p(z^*, t^*)\Delta t_+. \tag{46}$$

Since the constitutive equation (eqn (29)) requires information on both W^p and $\dot{W}^p$ to enable the determination of $\tau(z^*, t^* + \Delta t_+)$, an additional equation is needed. Accordingly, eqn (29) is differentiated with respect to time and used with eqn (28) to obtain

$$\overset{\circ\circ}{W}{}^p = \left\{\frac{2\tau - \kappa\,\mathrm{sgn}(\tau)}{\tau_0/\gamma_0}\right\} G(v' - \dot{W}^p/\tau) - \frac{|\tau|(\mathrm{d}\kappa/\mathrm{d}W^p)\dot{W}^p}{(\tau_0/\gamma_0)} \quad (|\tau| > \kappa, \dot{W}^p > 0). \tag{47}$$

A counterpart of eqn (46) is then written for $\dot{W}^p(z^*, t^* + \Delta t_+)$:

$$\dot{W}^p(z^*, t^* + \Delta t_+) = \dot{W}^p(z^*, t^*) + \overset{\circ\circ}{W}{}^p(z^*, t^*)\Delta t_+. \tag{48}$$

Equations (46), (48) and (29) provide enough information to solve for $\tau(z^*, t^* + \Delta t_+)$.

In order to calculate the reflected and transmitted waves at the left and right interfaces, the centered difference of eqn (23) is used at time $(t^* + \Delta t_+/2)$ and half of the spatial step away from the interface inside the specimen. The space-time grid used is shown in Fig. 5. Thus, the centered difference representation of eqn (23) is

$$\frac{\rho}{\Delta t_+}\left\{\begin{array}{l}\frac{1}{2}(v(z^*, t^* + \Delta t_+) + v(z^* + \Delta z_+, t^* + \Delta t_+)) \\ -\frac{1}{2}(v(z^*, t^*) + v(z^* + \Delta z_+, t^*))\end{array}\right\}$$
$$= \frac{1}{\Delta z_+}\left\{\begin{array}{l}\frac{1}{2}(\tau(z^* + \Delta z, t^* + \Delta t_+) + \tau(z^* + \Delta z_+, t^*)) \\ -\frac{1}{2}(\tau(z^*, t^* + \Delta t_+) + \tau(z^*, t^*))\end{array}\right\}. \tag{49}$$

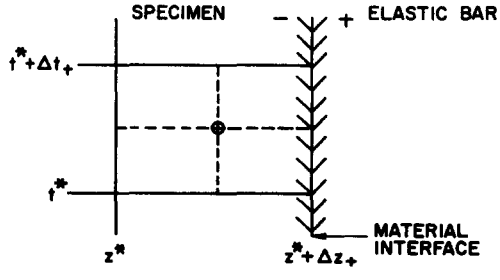

Fig. 5. Schematic of grid used with eqn (49).

Since the time derivative discontinuities at the interface are given by

$$[\mathring{\tau}] = [\mathring{\tau}]_{RT-} + [\mathring{\tau}]_{LT-}$$
$$[\mathring{v}] = [\mathring{v}]_{RT-} + [\mathring{v}]_{LT-}, \tag{50}$$

the reflected and transmitted stress and velocity waves are calculated by means of eqns (34) and (37) in conjunction with eqns (49) and (50).

To minimize computation time, a coarse spatial mesh was selected; the specimen length h was subdivided into five equal parts ($\Delta z_+ = \Delta z_- = h/5$). For stability in the numerical program, the time increment should satisfy

$$\Delta t \leq \Delta z/c \tag{51}$$

where c is given by the appropriate form of eqn (40). The maximum value of Δt was chosen to minimize run times. For the rate-independent material, c decreases from c_2 as plastic work increases.

The flow chart for the numerical program which implements the equations in this section is shown in Fig. 6. For listing and more details of the program, the reader is referred to Ref. [17].

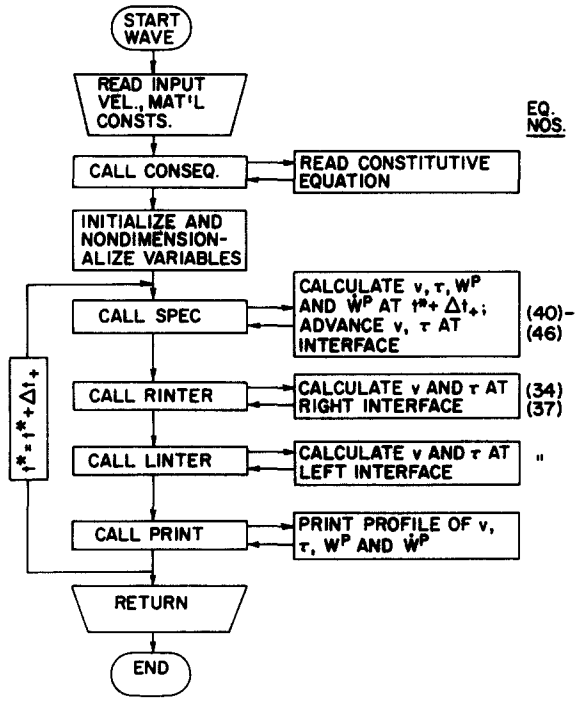

Fig. 6. Flow chart of wave program.

7. RESULTS

The experimental data of Duffy *et al.*[10] were used as a basis of comparison with the numerical program described in the previous sections. As input condition for the program, the incident stress history by Duffy was used; the predicted behavior of the reflected and transmitted stress history was then compared with the data reported by Duffy. Results are shown in Figs. 7 and 8, where the solid line represents the experimental data and the dashed and dot-dashed lines represent the predictions based on the viscoplastic model and the rate-independent plastic model, respectively. The value of the viscoplastic parameter τ_0/γ_0 used in the computation to give the best fit is $(80)^{-1}$ MPa·s. While this value is approximately 15% smaller than that predicted by the Kolsky data reduction formulas and reported in Section 3, it still provides rate-dependent hardening curves which lie within the experimental scatter (dashed lines, Fig. 2). For both the rate-independent and rate-dependent computations, the

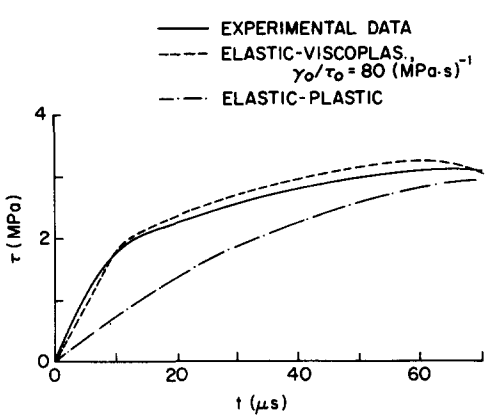

Fig. 7.

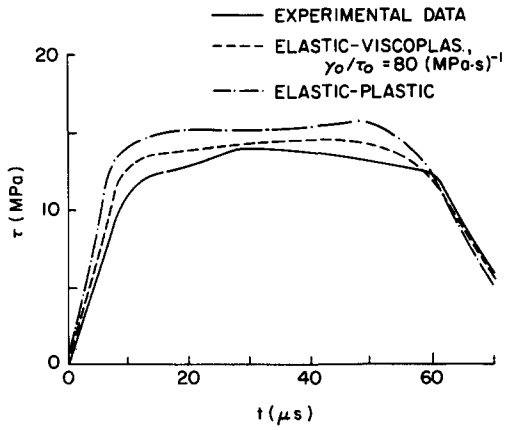

Fig. 8.

Fig. 7. Transmitted stress pulse from Duffy, Campbell and Hawley[10].
Fig. 8. Reflected stress pulse from Duffy, Campbell and Hawley[10].

elastic properties of the input and output bars were set at $G = 25.8$ GPa and $c_2 = 3.10$ mm$(\mu s)^{-1}$. Specimen length was $h = 2.71$ mm.

Agreement between predictions based on the rate-independent model and the measured data is rather poor. Although this agreement could be improved somewhat by replacing the $\mathring{W}^p = 0$ hardening curve with one for $\mathring{W}^p > 0$ (40 GPa·s^{-1}, for example), the amplitude rather than the shape of the predicted stress history would be influenced by such a change. As a result, the early time agreement would be achieved at the expense of agreement at the later times. Thus it appears that even an approximate hardening curve for the rate-independent model cannot achieve the overall agreement with the measured data of the type exhibited by the viscoplastic model.

Information on the plastic work accumulation within the specimen, $\bar{W}^p(t)$, is shown in Fig. 9 for both plastic and viscoplastic models. Although the shape of the curves is different for the

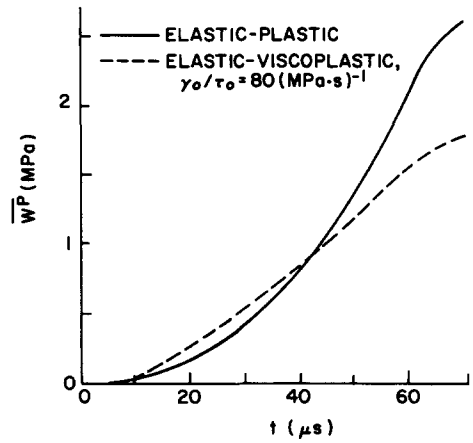

Fig. 9. $W^p(t)$ history in elastic-plastic and elastic-viscoplastic specimens.

two models, the order of magnitude is the same. Hence it is concluded that the overall amount of energy dissipated in the specimen is approximately the same, regardless of the mechanism (irreversible slip along preferred glide planes or viscous dissipation). Finally, in Fig. 10 stress profiles across the specimen are shown at different times throughout the passage of the pulse. At early times, some stress nonuniformity is evident; however, for times later than 10 μs, the profile is almost flat. After 60 μs, unloading begins as seen by the reduced amplitude of stress at $t = 70\ \mu$s.

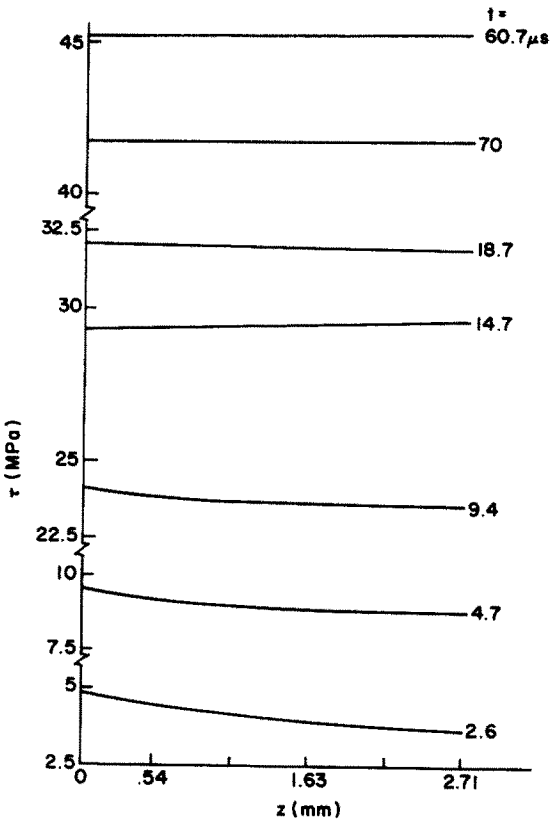

Fig. 10. Stress-profile in the specimen using elastic-viscoplastic program.

8. CONCLUSIONS

A computer program based on the method of singular surfaces has proved to be satisfactory for the calculation of weak wave propagation in elastic-plastic and elastic-viscoplastic solid-specimens sandwiched between two elastic bars (torsional Kolsky apparatus). It is found that a detailed analysis of propagation inside the specimen is necessary for accurate prediction of the material behavior because of departure from the stress-uniformity assumption used in arriving at the Kolsky formula for data reduction. Complete stress history of both reflected and transmitted pulses are needed. The rate-dependent constitutive relation gives excellent agreement between predicted histories and experimental data for Al 1100–0. Therefore, it is believed that Al 1100–0 is rate-dependent and the material behavior in pure shear can be well represented by Perzyna's elastic-viscoplastic model with the viscosity constant, (γ_0/τ_0), obtained by empirical fitting as 80 $(\text{MPa}\cdot\text{s})^{-1}$.

Acknowledgements—The work described here is based on part of doctoral thesis of the first author. We greatfully acknowledge the financial support by NSF Grant ENG-73-03525-A01.

REFERENCES

1. J. von Neumann and R. D. Richtmyer, A method for the numerical calculation of hydrodynamic shocks. *J. Appl. Phys.* **21**, 232–237 (1950).
2. R. Courant and K. O. Friedrichs, *Supersonic Flow and Shock Waves*. Interscience, New York (1948).
3. W. Herrmann and P. Holzhauser, *WONDY, A Computer Program for Calculating Problems of Motion in One Dimension*. SC-RR-66-601 (Feb. 1967).
4. S. F. Benzley, L. D. Bertholf and G. E. Clark, *Toody II-A, A Computer Program for Two Dimensional Wave Propagation—CDC 6600 Version*. Sandia Labs, SC-DR-69-516 (Nov. 1969).
5. R. Hill, Acceleration waves in solids. *J. Mech. Phys. Solids* **10**, 1–16 (1962).
6. D. M. Janssen, S. K. Datta and W. E. Jahsman, Propagation of weak waves in elastic-plastic solids. *J. Mech. Phys. Solids* **20**, 1–18 (1972).
7. W. E. Jahsman, Reflection and refraction weak elastic-plastic waves. *J. Appl. Mech.* **41**, (March 1974).
8. P. Perzyna, The constitutive equations for rate sensitive plastic materials. *Quart. Appl. Math.* **20**, 321–332 (1963).
9. L. E. Malvern, The propagation of longitudinal waves of plastic deformation in a bar of material exhibiting a strain-rate effect. *J. Appl. Mech.* 203–208 (1951).

10. J. Duffy, J. D. Campbell and R. H. Hawley, On the use of a torsional split Hopkinson bar to study rate effects in 1100–0 aluminium. *J. Appl. Mech.* **38**. 83–91 (1971).
11. T. Nicholas, Strain-rate and strain-rate history effects in several metals in torsion. *Experimental Mechanics* **11**, 370–374 (1971).
12. J. D. Campbell and A. R. Dowling, The behavior of materials subjected to dynamic incremental shear loading. *J. Mech. Phys. Solids* **18**, 43–63 (1970).
13. S. J. Green, F. L. Schierloh and S. G. Babcock, 1969 (results reported by Ref. [10]).
14. R. A. Frantz and J. Duffy, The dynamic stress-strain behavior in torsion of 1100–0 aluminium subjected to a sharp increase in strain rate. *J. Appl. Mech.* **39**, 939–945 (1972).
15. H. Kolsky, An investigation of the mechanical properties of materials at very high rates of loading. *Proc. Phys. Soc., Series B*, **62**, 676–700 (1949).
16. R. Hill, *The Mathematical Theory of Plasticity*. Oxford Univ. Press, London (1950).
17. B. Bhushan, Experimental and numerical studies of rate-dependent materials. Ph.D. Thesis, University of Colorado, Boulder (April 1976).